

62 64741 Copy 381  
RM A58C20

NACA RM A58C20

GPO PRICE \$ \_\_\_\_\_

OTS PRICE(S) \$ \_\_\_\_\_



Hard copy (HC) 2.50

Microfiche (MF) .50

# RESEARCH MEMORANDUM

AN EXPERIMENTAL INVESTIGATION OF THE STATIC LONGITUDINAL  
STABILITY AND CONTROL CHARACTERISTICS OF A  
WINGLESS MISSILE CONFIGURATION AT  
MACH NUMBERS FROM 3.0 TO 6.3

By Hermilo R. Gloria

Ames Aeronautical Laboratory  
Moffett Field, Calif.

DECLASSIFIED - EFFECTIVE 1-15-64  
Authority: Memo Geo. Drobka NASA HQ.  
Code ATSS-A Dtd. 3-12-64 Subj: Change  
in Security Classification Marking.

NATIONAL ADVISORY COMMITTEE  
FOR AERONAUTICS

WASHINGTON

June 24, 1958

N65-12702

(ACCESSION NUMBER)

(THRU)

(PAGES)

(CODE)

(NASA CR OR TMX OR AD NUMBER)

(CATEGORY)

FORM 602

[REDACTED]

## NATIONAL ADVISORY COMMITTEE FOR AERONAUTICS

RESEARCH MEMORANDUMAN EXPERIMENTAL INVESTIGATION OF THE STATIC LONGITUDINAL  
STABILITY AND CONTROL CHARACTERISTICS OF A  
WINGLESS MISSILE CONFIGURATION AT  
MACH NUMBERS FROM 3.0 TO 6.3

By Hermilo R. Gloria

## SUMMARY

Static longitudinal stability and control characteristics of a flare-stabilized body of revolution employing a movable portion of the flare surface as a pitch control were determined at Mach numbers from 3.00 to 6.28, angles of attack up to  $18^\circ$ , and control deflections up to  $40^\circ$ . Reynolds numbers (based on body length) varied from 9.4 million at  $M = 3.00$  to 1.8 million at  $M = 6.28$ . The test configuration consisted of a fineness-ratio-5 minimum-drag nose, a fineness-ratio-5 cylindrical mid-section, and a conical tail flare. The stabilizing flare consisted of a frustum of a fineness-ratio-5 cone extending two diameters forward of the base and increasing the base diameter by a factor of  $\sqrt{2}$ .

The variation of lift coefficient with pitching-moment coefficient for the basic configuration with control undeflected was found to be essentially linear, and the stability to increase slightly with increasing Mach number. Control effectiveness was essentially independent of Mach number at zero angle of attack but was found to decrease with increasing angle of attack. This decrease was due mostly to the shadowing of the control from the free stream by the forward part of the configuration, since the control surface was located entirely on the lee side of the configuration. At the higher test Mach numbers, additional losses in control effectiveness were noted which were caused by boundary-layer separation over the controls. These losses were associated, in part, with low test Reynolds numbers at the higher test Mach numbers.

For a given control deflection, trim lift coefficients decreased with increasing Mach number as a result of the loss in control effectiveness and an increase in stability of the basic configuration. Maximum

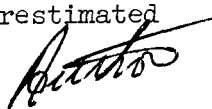
[REDACTED]

DECLASSIFIED - EFFECTIVE 1-25-64  
Authority: Memo Geo. Drobka NASA HQ.  
Code ATSS-A Dtd. 3-12-64 Subj: Change  
in Security Classification Marking

12702-over

trim lift-drag ratios between 2 and 2.5 were obtained and were about 30 percent lower than the maximum lift-drag ratios of the basic configuration.

At zero angle of attack, predictions with impact theory were found to be in good agreement with experimental results for incremental forces due to control deflection. At angle of attack, however, impact theory underestimated control effectiveness at low Mach numbers and overestimated effectiveness at high Mach numbers.




## INTRODUCTION

In the study of missile configurations suitable for flight at hypersonic speeds, considerable attention has been given to the wingless or all-body missile (see, e.g., refs. 1, 2, 3, and 4). Among the advantages attributed to these configurations are (1) a less severe problem of aerodynamic heating because of the absence of thin planar surfaces; and (2) aerodynamic force characteristics which tend to be independent of Mach number. In reference 1, a wingless configuration was studied which was stabilized by a conical flare at the base with control provided by deflectable sections of the body surface forward of the stabilizing flare. While the aerodynamic characteristics of this configuration compared favorably with those of a configuration employing planar surfaces for stability and control, the wingless missile tested did display certain undesirable properties. Among these are relatively low aerodynamic efficiency (i.e., lift-drag ratio) and reduced control effectiveness at low control deflection due to control-flare interference. Suggestions given in reference 1 for remedying these difficulties were that a more slender nose and stabilizing flare be employed to reduce drag and increase lift-drag ratio; to improve control effectiveness, it was suggested that the control surfaces be incorporated as part of the stabilizing flare. A configuration embodying these suggestions is the subject of the present report.

Force and moment characteristics as well as control forces are obtained for various flap deflections at Mach numbers from 3.00 to 6.28. Experimentally determined forces are compared with predictions of theory.

## NOTATION


- A      cross-sectional area of cylindrical mid-body, sq in.
- A<sub>c</sub>    control-surface plan area, sq in.
- C<sub>D</sub>    drag coefficient,  $\frac{\text{drag}}{qA}$
- 

- $C_h$  control hinge-moment coefficient about control leading edge,  
 $\frac{\text{hinge moment}}{qA_c l_f}$
- $C_L$  lift coefficient,  $\frac{\text{lift}}{qA}$
- $C_m$  pitching-moment coefficient about 0.47l,  $\frac{\text{pitching moment}}{qAl}$
- $C_N$  normal-force coefficient,  $\frac{\text{normal force}}{qA}$
- $C_{N_f}$  control normal-force coefficient (normal to control surface),  
 $\frac{\text{control normal force}}{qA_c}$
- d diameter of cylindrical mid-body, in.
- l body length, in.
- $l_f$  control surface length, in.
- M free-stream Mach number
- q free-stream dynamic pressure
- $\alpha$  angle of attack, deg
- $\delta$  control deflection angle, measured from flare surface, deg

## APPARATUS AND TESTS

Tests were conducted in the Ames 10- by 14-inch supersonic wind tunnel, which is described in detail in reference 5. Aerodynamic forces and moments acting on the test model were measured by strain-gage balances. The model was supported from the rear by a sting that was shrouded to within 0.040 inch of the model base, thereby eliminating, for all practical purposes, aerodynamic loads on the supports. Base pressures were measured in all tests and the resultant base forces (referred to free-stream static pressure) were subtracted from the measured axial forces.

Principal dimensions of the test model are shown in figure 1. The body of the configuration consists of three sections. The nose section is a minimum-drag body for given length and volume having a fineness ratio of 5 (ref. 6). Coordinates of the nose section are given in table I. The middle section is cylindrical and also has a fineness ratio



of 5. The flared tail section is a frustum of a fineness-ratio-5 cone, two cylinder diameters long, that increases the mid-body diameter by 1.41. The control surface is a portion of the top of the flare surface, 0.71 cylinder diameters wide, and it extends the full length of the tail flare. It is deflected above the flare surface from a hinge line located at the cylinder-flare juncture.

Tests were conducted at Mach numbers of 3.00, 4.24, 5.05, and 6.28, angles of attack up to  $18^\circ$ , and control deflections up to  $40^\circ$  above the flare surface. The free-stream Reynolds numbers based on body length are as follows:

<u>M</u>	<u>Reynolds number, millions</u>
3.00	9.36
4.24	8.64
5.05	4.20
6.28	1.80


Variations in free-stream Mach number did not exceed  $\pm 0.02$  at Mach numbers from 3.00 to 5.05 and  $\pm 0.04$  at  $M = 6.28$ . Deviations in free-stream Reynolds number did not exceed  $\pm 50,000$  from the values given previously. The estimated error in angle of attack and control deflection did not exceed  $\pm 0.2^\circ$ .

Precision of the experimental results is affected by uncertainties in measured forces, moments, and base pressures as well as in the determination of free-stream dynamic pressure and angle of attack. These uncertainties resulted in maximum possible errors in the aerodynamic force and moment coefficients as shown in the following table:

$C_L$	$\pm 0.03$
$C_D$	$\pm .03$
$C_m$	$\pm .04$
$C_h$	$\pm .02$
$C_{N_f}$	$\pm .02$

## RESULTS AND DISCUSSION

Experimental results of the present investigation are given in table II for the complete range of test variables. Portions of these data are also presented in graphical form in figures 2 through 6.



## Control-Body Combination Characteristics

The variations of lift coefficient with angle of attack, drag coefficient, and pitching-moment coefficient are presented in figure 2 for control deflections of  $0^\circ$ ,  $20^\circ$ , and  $40^\circ$  and for all four test Mach numbers. For the basic configuration ( $\delta = 0^\circ$ ), the variation of lift coefficient with angle of attack is seen to be relatively independent of Mach number. Similarly, the stability characteristics of the basic configuration, as demonstrated by the variation of lift coefficient with pitching-moment coefficient, show only a small change with Mach number. For example, the aerodynamic center moves only slightly rearward from 51 percent of the body length aft of the nose at  $M = 3.00$  to 54 percent at  $M = 6.28$ . In addition, the stability characteristics of the basic configuration are essentially linear. When the control is deflected, however, the stability characteristics become more nonlinear and there is a greater variation in aerodynamic characteristics with Mach number, indicating changes in control effectiveness.

## Control Effectiveness

The variations of lift, pitching-moment, and drag coefficients with control deflections are presented in figure 3 for all test Mach numbers and for several angles of attack. At zero angle of attack, the effect of the body flap control on  $C_L$ ,  $C_m$ , and  $C_D$  is maintained throughout the test range of control deflections. At this angle of attack, the control does not show the marked decrease in effectiveness with increasing Mach number that is so characteristic of planar controls; in fact, a small increase in effectiveness is indicated at the larger control deflections. When the configuration is inclined, however, there is a loss in control effectiveness, particularly at the smaller control deflections. This loss is more pronounced both at higher angles of attack and at higher Mach numbers. At  $M = 6.28$  and  $\alpha = 15^\circ$ , for example, the control is virtually ineffective throughout the test range of control deflections. Part of the loss in control effectiveness with angle of attack is undoubtedly due to the fact that the control is shadowed from the free stream by the forward part of the configuration, since the control is located on the top surface of the flare. Thus, the control operates in the wake of the body or at least in a region of reduced dynamic pressure.<sup>1</sup>

<sup>1</sup>A simple method for increasing the attractiveness of the body-flap control at angle of attack would involve the use of a flap on the lower surface of the stabilizing flare coupled to the upper flap so as to retract into the flare as the upper control is extended. Such a system would tend to reduce control hinge moments as well as increase effectiveness by reducing the stabilizing influence of the flare. This method was suggested in reference 1 and a similar configuration was investigated in reference 7. The present configuration did not involve the use of coupled flaps because of the limit in lower control travel imposed by the small flare angle.



While this effect would tend to increase with Mach number, it is not the only factor that would tend to reduce control effectiveness at the higher test Mach numbers. An additional loss is attributed to boundary-layer separation ahead of the control due, in part, to the lower test Reynolds numbers at the higher test Mach numbers. For a better understanding of this phenomenon, a visual study was made of the flow in the region of the control surface.

### Flow-Visualization Studies

Spark shadowgraphs of the flow in the region of the control surface are presented in figure 4 for control deflections of  $20^\circ$  and  $40^\circ$ , angles of attack of  $0^\circ$ ,  $7^\circ$ , and  $14^\circ$ , and Mach numbers of 4.24 and 5.05. The photographs for  $M = 4.24$  (figs. 4(a), (b), and (c)) are similar to those obtained for  $M = 3.00$  and they show flow in the region of the control that is typical of the flow that occurs when there is little or no boundary-layer separation. In these cases, the body boundary layer is turbulent ahead of the body-control juncture and it passes through the shock wave produced by the control without appreciable separation. In contrast, at  $M = 5.05$  (figs. 4(d), (e), and (f)) where the test Reynolds number is lower, the boundary layer is laminar ahead of the body-control juncture and extensive regions of separation occur. At angles of attack of  $7^\circ$  and  $14^\circ$ , for example, the separated region tends to envelope a large portion of the control surface. Similar photographs for  $M = 6.28$ , where the test Reynolds number is still lower, showed regions of separation which were even more extensive than those found at  $M = 5.05$ . It is apparent that if the flow over the control is separated, then the effectiveness of the control will be markedly reduced. Thus the photographs shown in figure 4 tend to explain the added loss in control effectiveness at high Mach numbers mentioned in the previous section. It should be noted, however, that the extent of flow separation is strongly dependent on the location of transition and thus on the Reynolds number (see ref. 8). At higher test Reynolds numbers, the region of separated flow would undoubtedly be smaller, but it would not be expected to disappear. In any event, it is evident that boundary-layer separation can have large effects on the stability and control characteristics of configurations which employ flares for stability and deflectable body segments for control. In this connection, it should be noted that part of the rearward movement of aerodynamic center at the higher Mach numbers mentioned previously can also be associated with the effects of separation ahead of the stabilizing flare (see ref. 9).

### Control Forces and Moments

The variation of control normal-force and hinge-moment coefficients with control deflection are presented in figures 5 and 6. In general,



these data corroborate the control-effectiveness results. For example, the variations of control normal-force and hinge-moment coefficients with control deflection at  $\alpha = 0^\circ$  are relatively independent of Mach number. In addition, at higher angles of attack and at the higher Mach numbers, the reduction in forces and moments experienced by the control is clearly evident. It should also be noted, however, that since the control has no aerodynamic balance, the hinge-moment coefficients are relatively large, at least when the control is effective. These large hinge moments may not necessarily be as big a disadvantage as for a wing trailing-edge control, however, since the mechanical problems associated with actuating the control will be reduced as a result of the location of the control.

### Trim Characteristics

From the results presented previously, the aerodynamic characteristics of the control-body combination in trimmed flight have been determined. In the determination of these characteristics, the center of gravity was assumed to be located at 47 percent of the body length aft of the nose. With this location, the static margin varies from  $1/8$  body diameter at  $M = 3.00$  to  $1/2$  body diameter at  $M = 6.28$ . For the selected center-of-gravity location, the aerodynamic characteristics of the trimmed configuration are shown as a function of Mach number for several control deflections in figure 7. One of the most pronounced trends evident in this figure is the decrease with increasing Mach number in trim lift coefficient and angle of attack that can be obtained with a given control deflection. For example, with a control deflection of  $40^\circ$ , the trim lift coefficient and angle of attack decrease from about 2.5 and  $22^\circ$ , respectively, at  $M = 3.00$  to about 1.0 and  $11^\circ$ , respectively, at  $M = 6.28$ . (Note that the trim point at  $M = 3.00$  was beyond the range of experimental results and was estimated by extrapolation of the data to higher angles of attack.) A large part of this reduction is, of course, associated with the loss in control effectiveness previously discussed; however, the increase in stability with Mach number is also a factor. Trim lift-drag ratios are shown as a function of Mach number for various control deflections in figure 8. It is noted that the highest ratios, between 2 and 2.5, are obtained with  $10^\circ$  control deflection. These values are about 30 percent lower than the maximum lift-drag ratios of the untrimmed basic configuration.

### Comparisons With Theoretical Predictions

The incremental lift and drag coefficients due to control deflection,  $\Delta C_L$  and  $\Delta C_D$ , have been estimated with the aid of impact theory (see, e.g., ref. 10). These estimates are compared with experimental results for several angles of attack at  $M = 3.00$  and  $M = 6.28$  in figure 9. In



application of the theory, the shadowing effect of the forebody on the control was considered by assuming zero pressure coefficient on portions of the control shielded from the air stream by the projection of the forebody at angle of attack. At zero angle of attack, the predictions of impact theory are in good agreement with experimental results. At  $M = 3.00$ , the control is more effective at angle of attack than is indicated by theory. It appears that at this Mach number, the forebody does not shadow the control to any appreciable extent. At  $M = 6.28$ , the control is less effective at angle of attack than predicted theoretically. While the shadowing effect undoubtedly increases with Mach number, much of the discrepancy is associated with the effects of boundary-layer separation which were not considered in the theory.

#### SUMMARY OF RESULTS


Static longitudinal stability and control characteristics of a flare-stabilized body of revolution employing a portion of the flare surface as a pitch control have been determined at Mach numbers from 3.00 to 6.28, angles of attack up to  $18^\circ$ , and control deflections up to  $40^\circ$ . Reynolds numbers (based on body length) varied from 9.4 million at  $M = 3.00$  to 1.8 million at  $M = 6.28$ . The results of this investigation are as follows:

1. For the basic configuration with control undeflected, the variation of lift coefficient with pitching-moment coefficient is essentially linear and stability increases slightly with increasing Mach number.

2. At zero angle of attack, control effectiveness is maintained throughout the test range of control deflections and it is essentially independent of Mach number. When the configuration is inclined, control effectiveness is decreased. Part of the loss in effectiveness is due to shadowing of the control from the free stream by the body of the configuration. Additional losses in control effectiveness occur at the higher test Mach numbers as a result of separation of the boundary layer ahead of the control. This separation is associated with the low test Reynolds numbers at the higher test Mach numbers.

3. For a given control deflection, trim lift coefficients decrease with increasing Mach number because of losses in control effectiveness and because of an increase in the stability of the basic configuration. Trim lift-drag ratios between 2 and 2.5 can be obtained with the test configuration. These values are about 30 percent lower than the ratios for the untrimmed basic configuration.

4. Incremental forces due to control deflection can be estimated at zero angle of attack by the use of impact theory. At angle of attack,



however, impact theory tends to underestimate control effectiveness at low Mach numbers and overestimates control effectiveness at high Mach numbers.

Ames Aeronautical Laboratory  
National Advisory Committee for Aeronautics  
Moffett Field, Calif., Mar. 20, 1958

#### REFERENCES

1. Eggers, A. J., Jr., and Syvertson, Clarence A.: Experimental Investigation of a Body Flare for Obtaining Pitch Stability and a Body Flap for Obtaining Pitch Control in Hypersonic Flight. NACA RM A54J13, 1955.
2. Lessing, Henry C., and Reese, David E., Jr.: A Simulation Study of a Wingless Missile. NACA RM A55L06, 1956.
3. Becker, J. V., and Korycinski, Peter F.: Heat Transfer and Pressure Distribution at a Mach Number of 6.8 on Bodies With Conical Flares and Extensive Flow Separation. NACA RM L56F22, 1956.
4. Penland, Jim A., and Carroll, C. Maria: Static Longitudinal and Lateral Stability Parameters of Three Flared-Skirt Two-Stage Missile Configurations at a Mach Number of 6.86. NACA RM L57D15, 1957.
5. Eggers, A. J., Jr., and Nothwang, George J.: The Ames 10- by 14-Inch Supersonic Wind Tunnel. NACA TN 3095, 1954.
6. Eggers, A. J., Jr., Resnikoff, Meyer M., and Dennis, David H.: Bodies of Revolution Having Minimum Drag at High Supersonic Airspeeds. NACA Rep. 1306, 1957. (Supersedes NACA TN 3666)
7. Reese, David E., Jr.: A Wind-Tunnel Investigation of Several Wingless Missile Configurations at Supersonic Speeds. NACA RM A57J22, 1958.
8. Chapman, Dean R., Kuehn, Donald M., and Larson, Howard K.: Investigation of Separated Flows in Supersonic and Subsonic Streams With Emphasis on the Effect of Transition. NACA TN 3869, 1957.
9. Dennis, David H., and Syvertson, Clarence A.: Effects of Boundary-Layer Separation on Normal Force and Center of Pressure of a Cone-Cylinder Model With a Large Base Flare at Mach Numbers From 3.00 to 6.28. NACA RM A55H09, 1955.
10. Grimminger, G., Williams, E. P., and Young, G. B. W.: Lift on Inclined Bodies of Revolution in Hypersonic Flow. Jour. Aero. Sci., vol. 17, no. 11, Nov. 1950, pp. 675-690.

03171254:30

TABLE I.- COORDINATES OF NOSE SECTION

Longitudinal station, x, in.	Radius, y, in.
0	0.0021
.1	.0352
.2	.0562
.3	.0749
.4	.0930
.6	.1262
.8	.1565
1.20	.2108
1.60	.2595
2.00	.3030
2.40	.3531
2.80	.3789
3.20	.4114
3.60	.4402
4.00	.4642
4.40	.4831
4.80	.4961
5.00	.5000

TABLE II.- EXPERIMENTAL RESULTS FOR THE FLARED-BODY BODY-FLAP COMBINATION

$\delta$ , deg	$\alpha$ , deg	$C_L$	$C_D$	$C_M$	$C_N$	$C_{N_f}$	$C_h$	$\delta$ , deg	$\alpha$ , deg	$C_L$	$C_D$	$C_M$	$C_N$	$C_{N_f}$	$C_h$	$\delta$ , deg	$\alpha$ , deg	$C_L$	$C_D$	$C_M$	$C_N$	$C_{N_f}$	$C_h$	
M = 3.00																								
0	-3.01	-0.1997	0.1552	0.0112	-0.2076	0.03498	0.01477	---	1.93	-0.9847	0.8116	0.3645	-0.5971	0.3815	0.2866	-30	10.03	1.0899	0.3592	-0.0783	1.1377	0.0928	0.0431	
-2.01	-1.183	-0.0763	0.076	0.0076	-0.1365	0.03420	0.01461	---	2.95	-0.5101	0.7850	0.3509	-0.4691	0.3608	0.2786	12.08	12.08	1.4519	0.4756	-0.1367	1.5193	0.0928	0.0431	
-4.01	-0.650	0.1162	0.035	0.0035	-0.0655	0.03367	0.01491	---	4.95	-0.2835	0.6664	0.3037	-0.4691	0.3608	0.2786	13.48	13.48	1.6218	0.4756	-0.1367	1.5193	0.0928	0.0431	
1.02	0.0604	0.1162	0.035	0.0035	-0.0655	0.03367	0.01491	---	6.95	-0.1162	0.6841	0.3022	-0.4691	0.3608	0.2786	15.24	15.24	1.7967	0.4756	-0.1367	1.5193	0.0928	0.0431	
2.03	0.1260	0.1162	0.035	0.0035	-0.0655	0.03367	0.01491	---	10.05	-0.0796	0.6959	0.2869	-0.4691	0.3608	0.2786	15.24	15.24	1.9811	0.4756	-0.1367	1.5193	0.0928	0.0431	
3.05	0.1944	0.1162	0.035	0.0035	-0.0655	0.03367	0.01491	---	12.17	0.0796	0.7043	0.2869	-0.4691	0.3608	0.2786	17.31	17.31	2.3116	0.4756	-0.1367	1.5193	0.0928	0.0431	
4.07	0.2617	0.1162	0.035	0.0035	-0.0655	0.03367	0.01491	---	13.24	0.2617	0.7043	0.2869	-0.4691	0.3608	0.2786	18.34	18.34	2.5311	0.4756	-0.1367	1.5193	0.0928	0.0431	
5.01	0.3177	0.1162	0.035	0.0035	-0.0655	0.03367	0.01491	---	14.40	0.2778	0.6986	0.2869	-0.4691	0.3608	0.2786	20	20	2.5311	0.4756	-0.1367	1.5193	0.0928	0.0431	
6.07	0.3694	0.1162	0.035	0.0035	-0.0655	0.03367	0.01491	---	15.47	0.2778	0.6986	0.2869	-0.4691	0.3608	0.2786	20	20	2.5311	0.4756	-0.1367	1.5193	0.0928	0.0431	
7.07	0.4196	0.1162	0.035	0.0035	-0.0655	0.03367	0.01491	---	17.62	0.2067	1.1945	0.3327	-0.4691	0.3608	0.2786	20	20	2.5311	0.4756	-0.1367	1.5193	0.0928	0.0431	
8.07	0.4694	0.1162	0.035	0.0035	-0.0655	0.03367	0.01491	---	18.69	0.2067	1.1945	0.3327	-0.4691	0.3608	0.2786	20	20	2.5311	0.4756	-0.1367	1.5193	0.0928	0.0431	
9.07	0.5196	0.1162	0.035	0.0035	-0.0655	0.03367	0.01491	---	20	20	2.5311	0.4756	-0.1367	1.5193	0.0928	0.0431	20	20	2.5311	0.4756	-0.1367	1.5193	0.0928	0.0431
10.07	0.5694	0.1162	0.035	0.0035	-0.0655	0.03367	0.01491	---	20	20	2.5311	0.4756	-0.1367	1.5193	0.0928	0.0431	20	20	2.5311	0.4756	-0.1367	1.5193	0.0928	0.0431
11.07	0.6196	0.1162	0.035	0.0035	-0.0655	0.03367	0.01491	---	20	20	2.5311	0.4756	-0.1367	1.5193	0.0928	0.0431	20	20	2.5311	0.4756	-0.1367	1.5193	0.0928	0.0431
12.07	0.6694	0.1162	0.035	0.0035	-0.0655	0.03367	0.01491	---	20	20	2.5311	0.4756	-0.1367	1.5193	0.0928	0.0431	20	20	2.5311	0.4756	-0.1367	1.5193	0.0928	0.0431
13.07	0.7196	0.1162	0.035	0.0035	-0.0655	0.03367	0.01491	---	20	20	2.5311	0.4756	-0.1367	1.5193	0.0928	0.0431	20	20	2.5311	0.4756	-0.1367	1.5193	0.0928	0.0431
14.07	0.7694	0.1162	0.035	0.0035	-0.0655	0.03367	0.01491	---	20	20	2.5311	0.4756	-0.1367	1.5193	0.0928	0.0431	20	20	2.5311	0.4756	-0.1367	1.5193	0.0928	0.0431
15.07	0.8196	0.1162	0.035	0.0035	-0.0655	0.03367	0.01491	---	20	20	2.5311	0.4756	-0.1367	1.5193	0.0928	0.0431	20	20	2.5311	0.4756	-0.1367	1.5193	0.0928	0.0431
16.07	0.8694	0.1162	0.035	0.0035	-0.0655	0.03367	0.01491	---	20	20	2.5311	0.4756	-0.1367	1.5193	0.0928	0.0431	20	20	2.5311	0.4756	-0.1367	1.5193	0.0928	0.0431
17.07	0.9196	0.1162	0.035	0.0035	-0.0655	0.03367	0.01491	---	20	20	2.5311	0.4756	-0.1367	1.5193	0.0928	0.0431	20	20	2.5311	0.4756	-0.1367	1.5193	0.0928	0.0431
18.07	0.9694	0.1162	0.035	0.0035	-0.0655	0.03367	0.01491	---	20	20	2.5311	0.4756	-0.1367	1.5193	0.0928	0.0431	20	20	2.5311	0.4756	-0.1367	1.5193	0.0928	0.0431
19.07	1.0196	0.1162	0.035	0.0035	-0.0655	0.03367	0.01491	---	20	20	2.5311	0.4756	-0.1367	1.5193	0.0928	0.0431	20	20	2.5311	0.4756	-0.1367	1.5193	0.0928	0.0431
20.07	1.0694	0.1162	0.035	0.0035	-0.0655	0.03367	0.01491	---	20	20	2.5311	0.4756	-0.1367	1.5193	0.0928	0.0431	20	20	2.5311	0.4756	-0.1367	1.5193	0.0928	0.0431
M = 4.24																								
-10	-3.09	-0.1997	0.1552	0.0112	-0.2076	0.03498	0.01477	---	1.93	-0.9847	0.8116	0.3645	-0.5971	0.3815	0.2866	-30	10.03	1.0899	0.3592	-0.0783	1.1377	0.0928	0.0431	
-2.07	-1.183	-0.0763	0.076	0.0076	-0.1365	0.03420	0.01461	---	2.95	-0.5101	0.7850	0.3509	-0.4691	0.3608	0.2786	12.08	12.08	1.4519	0.4756	-0.1367	1.5193	0.0928	0.0431	
-4.07	-0.650	0.1162	0.035	0.0035	-0.0655	0.03367	0.01491	---	4.95	-0.2835	0.6664	0.3037	-0.4691	0.3608	0.2786	13.48	13.48	1.6218	0.4756	-0.1367	1.5193	0.0928	0.0431	
-6.07	-0.1260	0.1162	0.035	0.0035	-0.0655	0.03367	0.01491	---	6.95	-0.1162	0.6841	0.3022	-0.4691	0.3608	0.2786	15.24	15.24	1.7967	0.4756	-0.1367	1.5193	0.0928	0.0431	
-8.07	0.0604	0.1162	0.035	0.0035	-0.0655	0.03367	0.01491	---	10.07	-0.0796	0.6959	0.2869	-0.4691	0.3608	0.2786	15.24	15.24	1.9811	0.4756	-0.1367	1.5193	0.0928	0.0431	
-10.07	0.1260	0.1162	0.035	0.0035	-0.0655	0.03367	0.01491	---	12.17	0.0796	0.7043	0.2869	-0.4691	0.3608	0.2786	17.31	17.31	2.3116	0.4756	-0.1367	1.5193	0.0928	0.0431	
-12.07	0.1944	0.1162	0.035	0.0035	-0.0655	0.03367	0.01491	---	13.24	0.2617	0.7043	0.2869	-0.4691	0.3608	0.2786	18.34	18.34	2.5311	0.4756	-0.1367	1.5193	0.0928	0.0431	
-14.07	0.2617	0.1162	0.035	0.0035	-0.0655	0.03367	0.01491	---	14.40	0.2778	0.6986	0.2869	-0.4691	0.3608	0.2786	20	20	2.5311	0.4756	-0.1367	1.5193	0.0928	0.0431	
-16.07	0.3177	0.1162	0.035	0.0035	-0.0655	0.03367	0.01491	---	15.47	0.2778	0.6986	0.2869	-0.4691	0.3608	0.2786	20	20	2.5311	0.4756	-0.1367	1.5193	0.0928	0.0431	
-18.07	0.3694	0.1162	0.035	0.0035	-0.0655	0.03367	0.01491	---	17.62	0.2067	1.1945	0.3327	-0.4691	0.3608	0.2786	20	20	2.5311	0.4756	-0.1367	1.5193	0.0928	0.0431	
-20.07	0.4196	0.1162	0.035	0.0035	-0.0655	0.03367	0.01491	---	18.69	0.2067	1.1945	0.3327	-0.4691	0.3608	0.2786	20	20	2.5311	0.4756	-0.1367	1.5193	0.0928	0.0431	
-22.07	0.4694	0.1162	0.035	0.0035	-0.0655	0.03367	0.01491	---	20	20	2.5311	0.4756	-0.1367	1.5193	0.0928	0.0431	20	20	2.5311	0.4756	-0.1367	1.5193	0.0928	0.0431
-24.07	0.5196	0.1162	0.035	0.0035	-0.0655	0.03367	0.01491	---	20	20	2.5311	0.4756	-0.1367	1.5193	0.0928	0.0431	20	20	2.5311	0.4756	-0.1367	1.5193	0.0928	0.0431
-26.07	0.5694	0.1162	0.035	0.0035	-0.0655	0.03367	0.01491	---	20	20	2.5311	0.4756	-0.1367	1.5193	0.0928	0.0431	20	20	2.5311	0.4756	-0.1367	1.5193	0.0928	0.0431
-28.07	0.6196	0.1162	0.035	0.0035	-0.0655	0.03367	0.01491	---	20	20	2.5311	0.4756	-0.1367	1.5193	0.0928	0.0431	20	20	2.5311	0.4756	-0.1367	1.5193	0.0928	0.0431
-30.07	0.6694	0.1162	0.035	0.0035	-0.0655	0.03367	0.01491	---	20	20	2.5311	0.4756	-0.1367	1.5193	0.0928	0.0431	20	20	2.5311	0.4756	-0.1367	1.5193	0.0928	0.0431
-32.07	0.7196	0.1162	0.035	0.0035	-0.0655	0.03367	0.01491	---	20	20	2.5311	0.4756	-0.1367	1.5193	0.0928	0.0431	20	20	2.5311	0.4756	-0.1367	1.5193	0.0928	0.0431
-34.07	0.7694	0.1162	0.035	0.0035	-0.0655	0.03367	0.01491	---	20	20	2.5311	0.4756	-0.1367	1.5193	0.0928	0.0431	20	20	2.5311	0.4756	-0.1367	1.5193	0.0928	0.0431
-36.07	0.8196	0.1162	0.035	0.0035	-0.0655	0.03367	0.01491	---	20	20	2.5311	0.4756	-0.1367	1.5193	0.0928	0.0431	20	20	2.5311	0.4756	-0.1367	1.5193	0.0928	0.0431
-38.07	0.8694	0.1162	0.035	0.0035	-0.0655	0.03367	0.01491	---	20	20	2.5311	0.4756	-0.1367	1.5193	0.0928	0.0431	20	20	2.5311	0.4756	-0.1367	1.5193	0.0928	0.0431
-40.07	0.9196	0.1162	0.035	0.0035	-0.0655	0.03367	0.01491	---	20	20	2.5311	0.4756	-0.1367	1.5193	0.0928	0.0431	20	20	2.5311	0.4756	-0.1367	1.5193	0.0928	0.0431
-42.07	0.96																							

TABLE II.- EXPERIMENTAL RESULTS FOR THE FLARED-BODY BODY-FLAP COMBINATION - Concluded

$\delta$ , deg	$\alpha$ , deg	$C_L$	$C_D$	$C_m$	$C_N$	$C_{Nf}$	$C_h$	$\delta$ , deg	$\alpha$ , deg	$C_L$	$C_D$	$C_m$	$C_N$	$C_{Nf}$	$C_h$
$M = 5.0$															
0	-3.02	-0.2535	0.1452	0.0229	-0.2608	---	---	0	0.97	-0.6696	0.7407	0.3816	-0.6571	0.3630	0.3044
-2.01	-1.697	-0.1897	0.1385	0.0164	-0.1744	0.03725	0.02214	-30	1.98	-0.5460	0.7073	0.3462	-0.5214	0.5202	0.2778
0	-0.862	0.1219	0	0.0091	-0.0885	0.03347	0.02022	-2.99	2.99	-0.4410	0.6678	0.3271	-0.5078	0.4881	0.2666
1.00	0.0769	0.1231	0.0009	0	0.0753	0.02880	0.01806	4.89	4.89	-1.563	0.5938	0.2707	-1.050	0.4662	0.2637
2.01	0.1669	0.1312	-0.0136	0.0091	-0.0753	0.02880	0.01866	6.91	6.91	0.995	0.5951	0.2309	-1.705	0.4184	0.2515
3.02	0.2325	0.1363	-0.0094	0.0091	-0.0753	0.02880	0.01866	7.93	7.93	0.995	0.5951	0.2309	-1.705	0.4184	0.2515
4.92	0.2982	0.1547	-0.0756	0.0091	-0.0753	0.02880	0.01866	9.92	9.92	0.995	0.5951	0.2309	-1.705	0.4184	0.2515
6.95	0.3566	0.1547	-0.0756	0.0091	-0.0753	0.02880	0.01866	11.96	11.96	1.152	0.6139	0.0956	-1.7730	0.3173	0.2066
7.96	0.3971	0.1659	-0.2537	0.0091	-0.0753	0.02880	0.01866	12.97	12.97	1.320	0.6693	0.0765	-1.7730	0.3173	0.2066
9.95	0.41745	0.1659	-0.2537	0.0091	-0.0753	0.02880	0.01866	14.06	14.06	1.607	0.8960	0.0765	-1.7730	0.3173	0.2066
11.97	0.41745	0.1659	-0.2537	0.0091	-0.0753	0.02880	0.01866	15.08	15.08	1.917	1.1318	0.0765	-1.7730	0.3173	0.2066
12.99	0.41745	0.1659	-0.2537	0.0091	-0.0753	0.02880	0.01866	13.13	13.13	2.3932	1.2230	0.2612	-2.4277	0.0773	0.04357
14.07	0.41745	0.1659	-0.2537	0.0091	-0.0753	0.02880	0.01866	14.06	14.06	1.994	1.1328	0.0765	-1.7730	0.3173	0.2066
15.08	0.41745	0.1659	-0.2537	0.0091	-0.0753	0.02880	0.01866	15.08	15.08	2.3932	1.2230	0.2612	-2.4277	0.0773	0.04357
16.12	0.41745	0.1659	-0.2537	0.0091	-0.0753	0.02880	0.01866	16.12	16.12	2.3932	1.2230	0.2612	-2.4277	0.0773	0.04357
17.13	0.41745	0.1659	-0.2537	0.0091	-0.0753	0.02880	0.01866	17.13	17.13	2.3932	1.2230	0.2612	-2.4277	0.0773	0.04357
18.13	0.41745	0.1659	-0.2537	0.0091	-0.0753	0.02880	0.01866	18.13	18.13	2.3932	1.2230	0.2612	-2.4277	0.0773	0.04357
$M = 5.0$															
-10	-3.03	-0.4479	0.2448	0.054	-0.4605	---	---	-40	-2.04	-1.198	0.1403	0.6139	-1.2477	0.9534	0.4798
-2.02	-2.54	-0.2812	0.2282	0.0907	-0.3633	0.2023	0.1076	-30	-1.04	-1.094	0.328	0.5805	-1.1178	0.9069	0.4574
-3.01	-2.072	-0.2031	0.0644	-0.2091	-0.2633	0.1850	0.0989	-2.99	2.99	-0.4410	0.6678	0.3271	-1.050	0.4662	0.2637
-4.91	-1.709	0.1936	0.0695	-0.1709	-0.1634	---	---	4.89	4.89	-1.563	0.5938	0.2707	-1.050	0.4662	0.2637
-5.91	-1.192	0.1911	0.0330	-0.1134	-0.0778	0.0937	0.0844	6.91	6.91	0.995	0.5951	0.2309	-1.705	0.4184	0.2515
-6.91	-0.011	0.1897	0.0013	-0.0078	-0.1448	0.0844	0.0844	7.93	7.93	0.995	0.5951	0.2309	-1.705	0.4184	0.2515
-7.93	0.002	0.1878	0.0520	-0.0107	-0.1278	0.078	0.0632	9.92	9.92	0.995	0.5951	0.2309	-1.705	0.4184	0.2515
-8.95	0.002	0.1878	0.0520	-0.0107	-0.1278	0.078	0.0632	11.96	11.96	1.152	0.6139	0.0956	-1.7730	0.3173	0.2066
-9.95	0.002	0.1878	0.0520	-0.0107	-0.1278	0.078	0.0632	12.97	12.97	1.320	0.6693	0.0765	-1.7730	0.3173	0.2066
-10.97	0.002	0.1878	0.0520	-0.0107	-0.1278	0.078	0.0632	14.06	14.06	1.607	0.8960	0.0765	-1.7730	0.3173	0.2066
-11.97	0.002	0.1878	0.0520	-0.0107	-0.1278	0.078	0.0632	15.08	15.08	1.917	1.1318	0.0765	-1.7730	0.3173	0.2066
-12.99	0.002	0.1878	0.0520	-0.0107	-0.1278	0.078	0.0632	13.13	13.13	2.3932	1.2230	0.2612	-2.4277	0.0773	0.04357
-14.07	0.002	0.1878	0.0520	-0.0107	-0.1278	0.078	0.0632	14.06	14.06	1.994	1.1328	0.0765	-1.7730	0.3173	0.2066
-15.08	0.002	0.1878	0.0520	-0.0107	-0.1278	0.078	0.0632	15.08	15.08	2.3932	1.2230	0.2612	-2.4277	0.0773	0.04357
-16.12	0.002	0.1878	0.0520	-0.0107	-0.1278	0.078	0.0632	16.12	16.12	2.3932	1.2230	0.2612	-2.4277	0.0773	0.04357
-17.13	0.002	0.1878	0.0520	-0.0107	-0.1278	0.078	0.0632	17.13	17.13	2.3932	1.2230	0.2612	-2.4277	0.0773	0.04357
-18.13	0.002	0.1878	0.0520	-0.0107	-0.1278	0.078	0.0632	18.13	18.13	2.3932	1.2230	0.2612	-2.4277	0.0773	0.04357
$M = 6.28$															
-20	-3.04	-0.7442	0.5343	0.2715	-0.7716	---	---	-30	-2.03	-1.195	0.9835	0.1915	-0.9835	0.1915	0.9835
-1.03	-2.514	-0.4629	0.2373	-0.5988	-0.4014	---	---	-2.99	-2.99	-0.4410	0.6678	0.3271	-1.050	0.4662	0.2637
-2.02	-2.072	-0.2031	0.0644	-0.2091	-0.2633	0.1850	0.0989	4.89	4.89	-1.563	0.5938	0.2707	-1.050	0.4662	0.2637
-3.01	-1.709	0.1936	0.0695	-0.1709	-0.1634	---	---	6.91	6.91	0.995	0.5951	0.2309	-1.705	0.4184	0.2515
-4.91	-1.192	0.1911	0.0330	-0.1134	-0.0778	0.0937	0.0844	7.93	7.93	0.995	0.5951	0.2309	-1.705	0.4184	0.2515
-5.91	-0.011	0.1897	0.0013	-0.0078	-0.1448	0.0844	0.0844	9.92	9.92	0.995	0.5951	0.2309	-1.705	0.4184	0.2515
-6.91	0.002	0.1878	0.0520	-0.0107	-0.1278	0.078	0.0632	11.96	11.96	1.152	0.6139	0.0956	-1.7730	0.3173	0.2066
-7.93	0.002	0.1878	0.0520	-0.0107	-0.1278	0.078	0.0632	12.97	12.97	1.320	0.6693	0.0765	-1.7730	0.3173	0.2066
-8.95	0.002	0.1878	0.0520	-0.0107	-0.1278	0.078	0.0632	14.06	14.06	1.607	0.8960	0.0765	-1.7730	0.3173	0.2066
-9.95	0.002	0.1878	0.0520	-0.0107	-0.1278	0.078	0.0632	15.08	15.08	1.917	1.1318	0.0765	-1.7730	0.3173	0.2066
-10.97	0.002	0.1878	0.0520	-0.0107	-0.1278	0.078	0.0632	13.13	13.13	2.3932	1.2230	0.2612	-2.4277	0.0773	0.04357
-11.97	0.002	0.1878	0.0520	-0.0107	-0.1278	0.078	0.0632	14.06	14.06	1.994	1.1328	0.0765	-1.7730	0.3173	0.2066
-12.99	0.002	0.1878	0.0520	-0.0107	-0.1278	0.078	0.0632	15.08	15.08	2.3932	1.2230	0.2612	-2.4277	0.0773	0.04357
-14.07	0.002	0.1878	0.0520	-0.0107	-0.1278	0.078	0.0632	16.12	16.12	2.3932	1.2230	0.2612	-2.4277	0.0773	0.04357
-15.08	0.002	0.1878	0.0520	-0.0107	-0.1278	0.078	0.0632	17.13	17.13	2.3932	1.2230	0.2612	-2.4277	0.0773	0.04357
-16.12	0.002	0.1878	0.0520	-0.0107	-0.1278	0.078	0.0632	18.13	18.13	2.3932	1.2230	0			

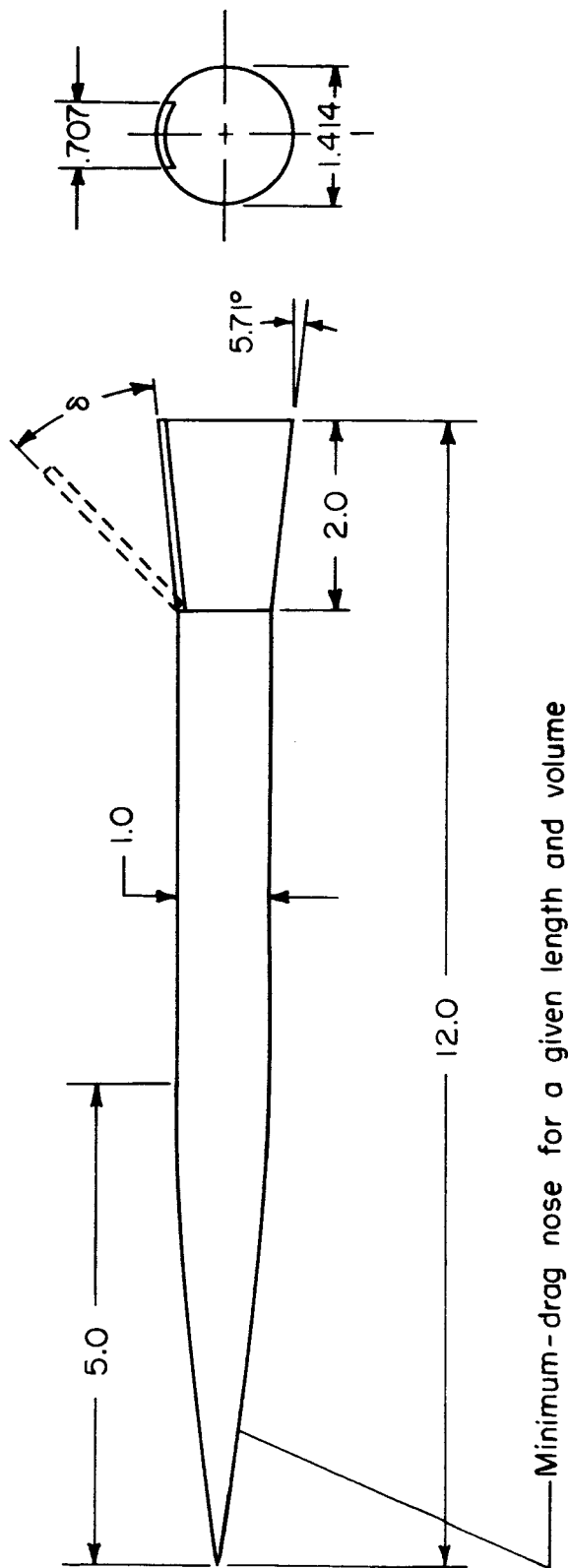


Figure 1.- Principal dimensions of test model.

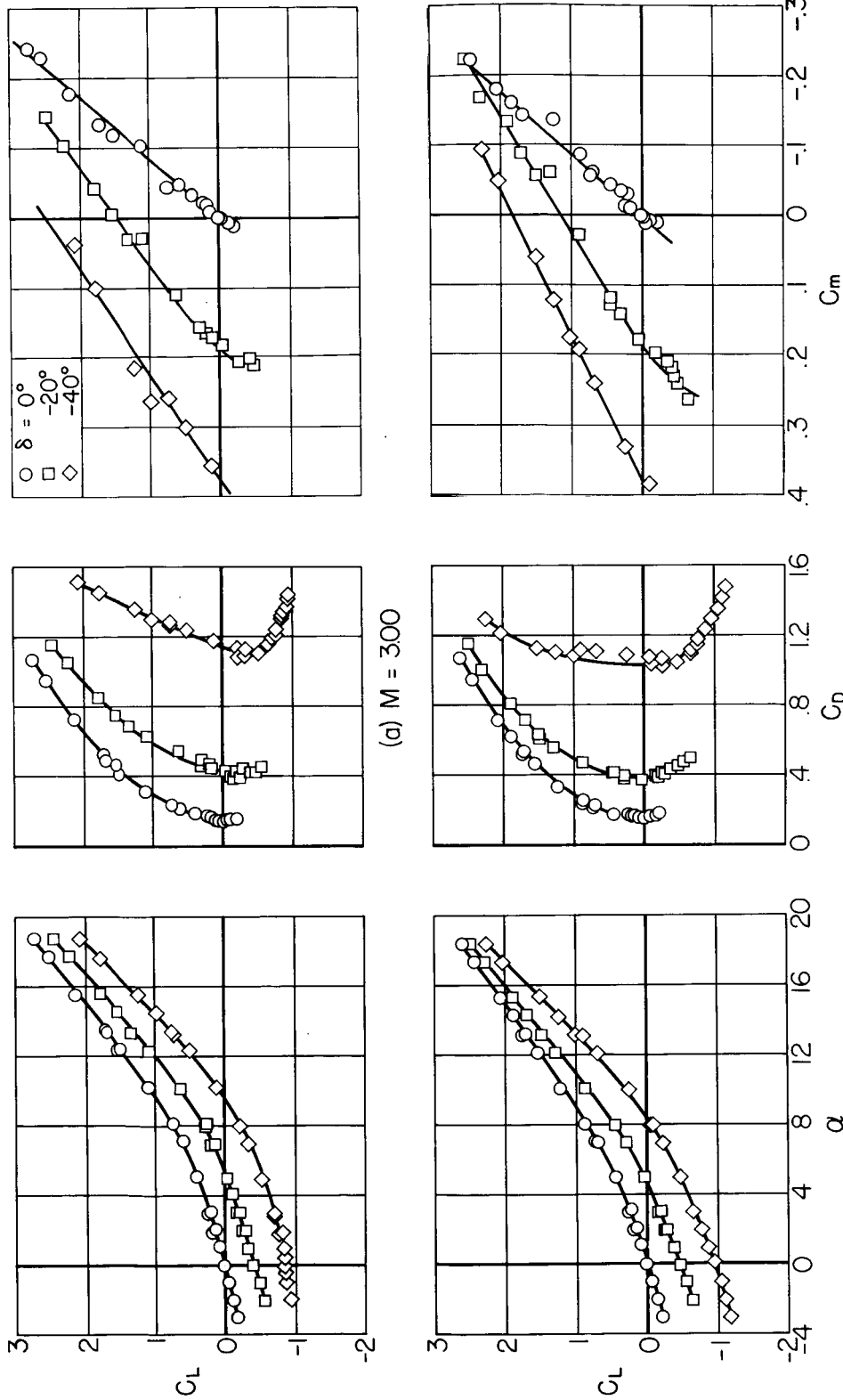
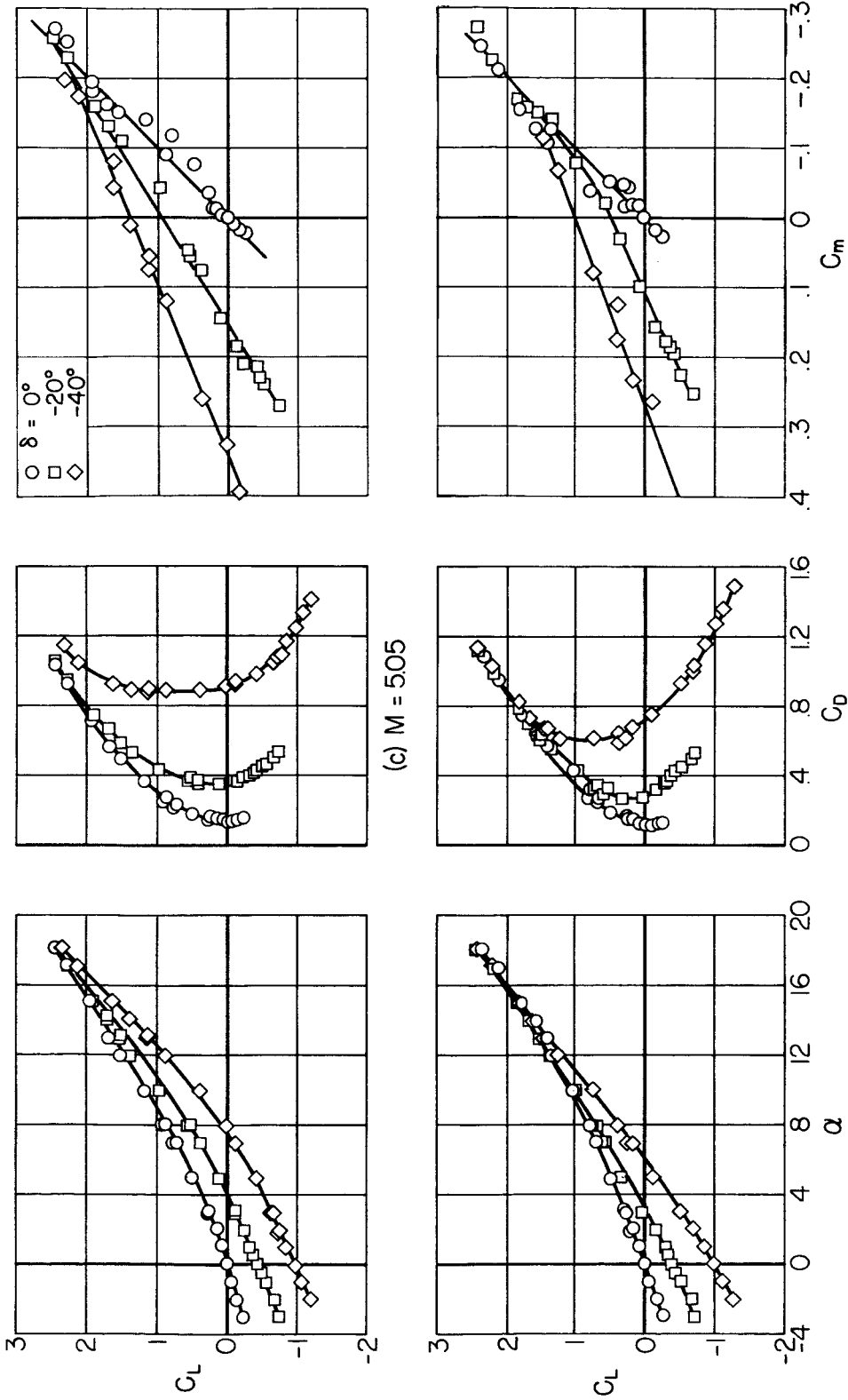


Figure 2.- Performance and longitudinal stability characteristics of the test configuration.



(d)  $M = 6.28$

Figure 2.- Concluded.



CONFIDENTIAL

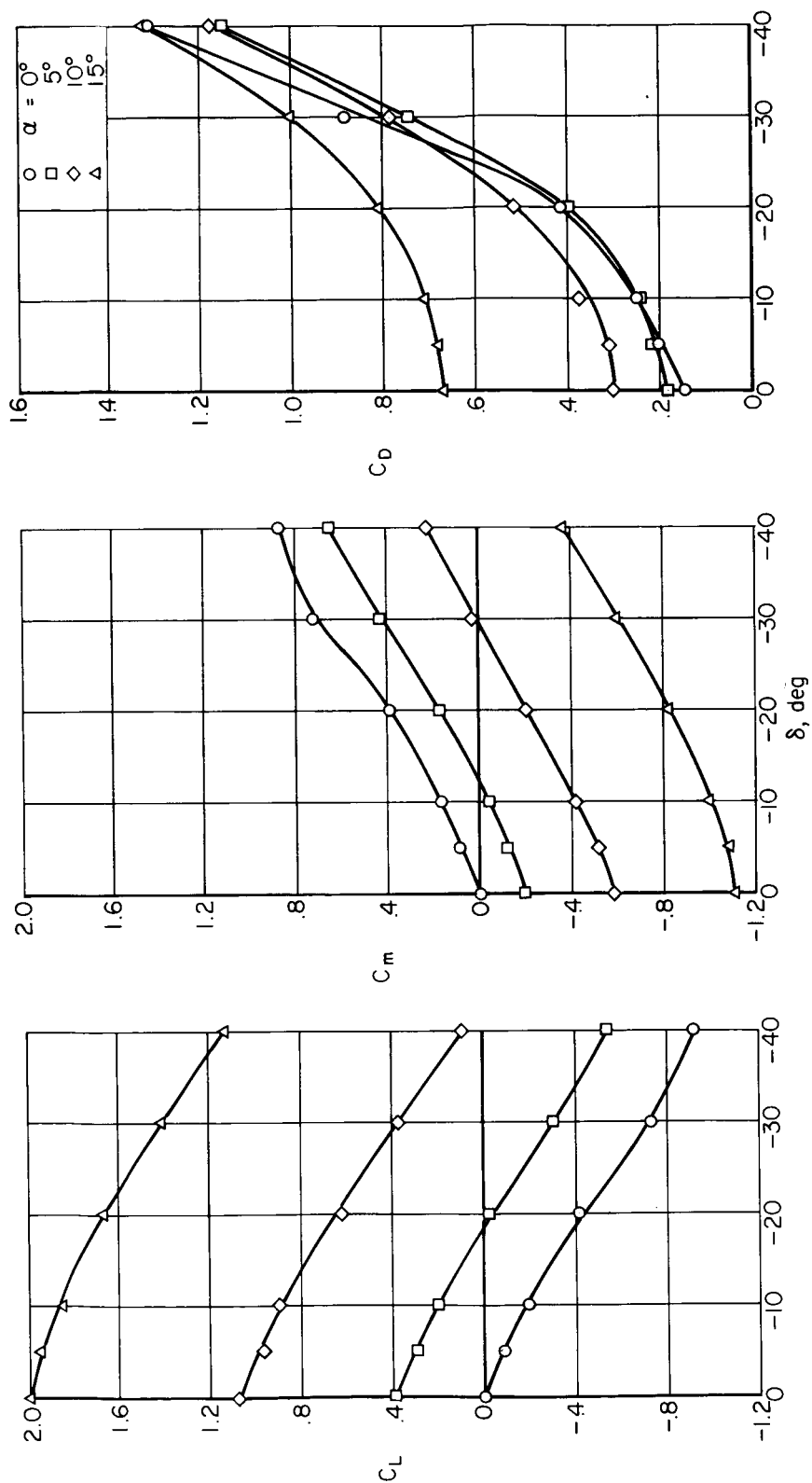
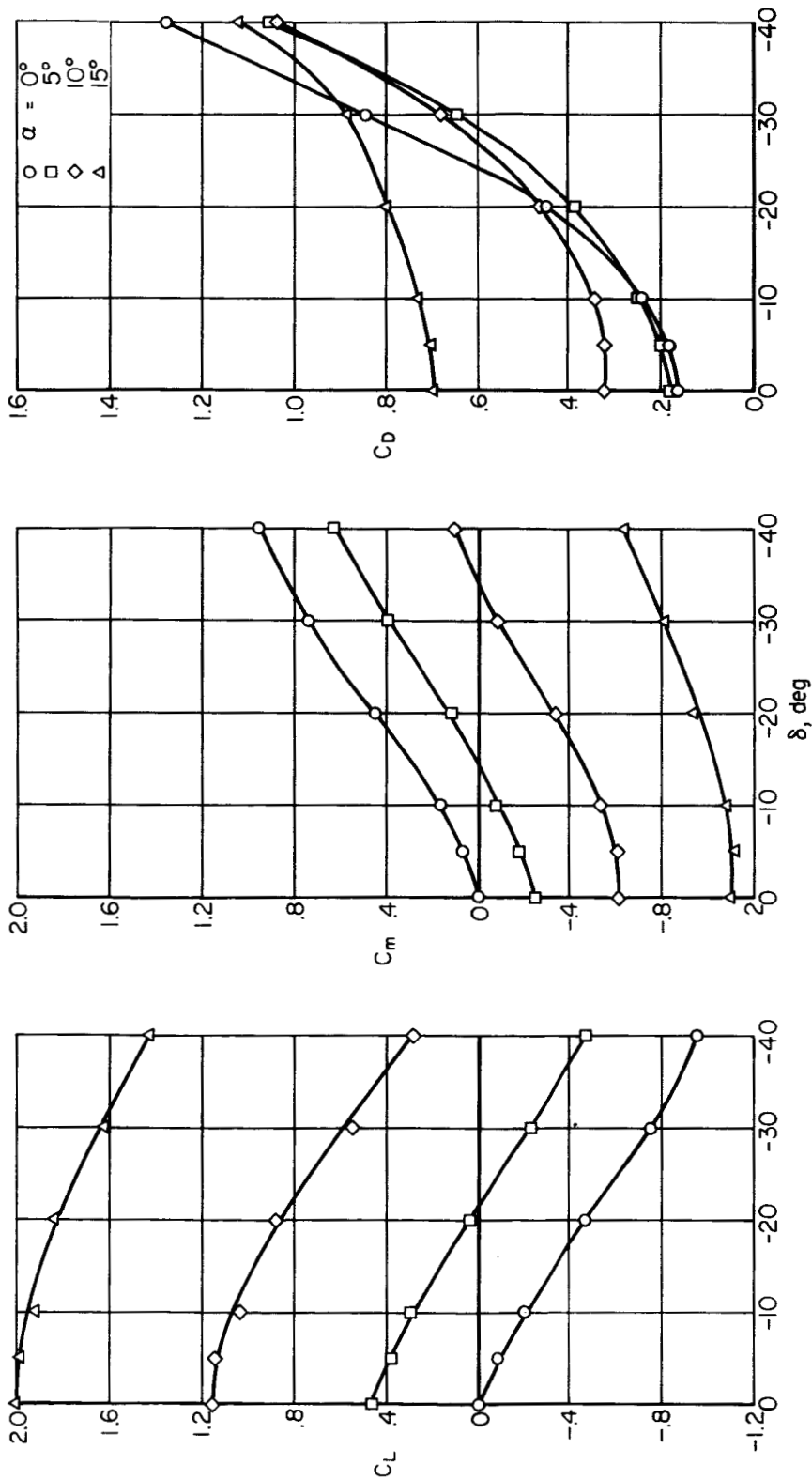
(a)  $M = 3.00$ 

Figure 3.- Variation of lift, pitching-moment, and drag coefficients with control deflection.



(b)  $M = 4.24$

Figure 3.- Continued.

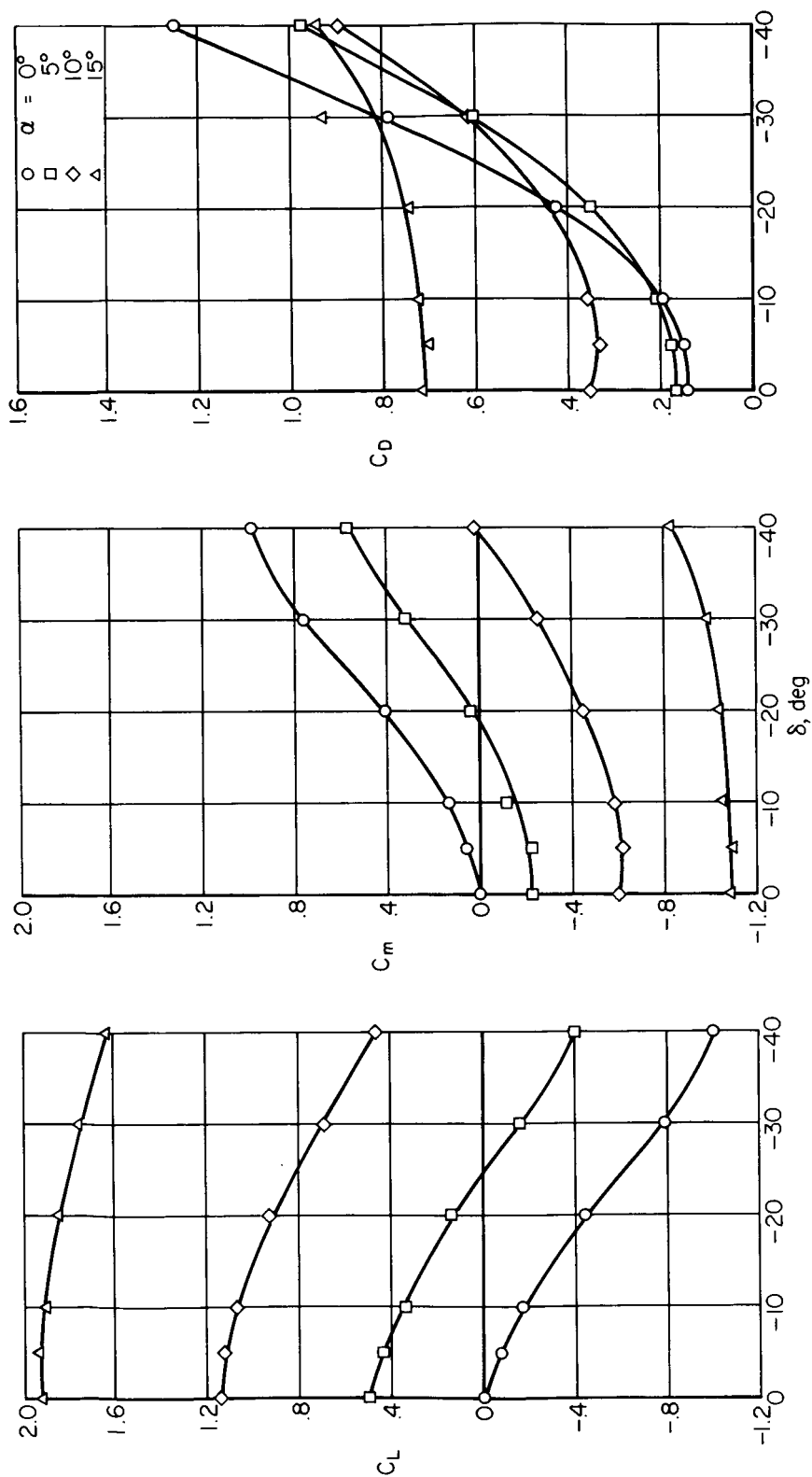
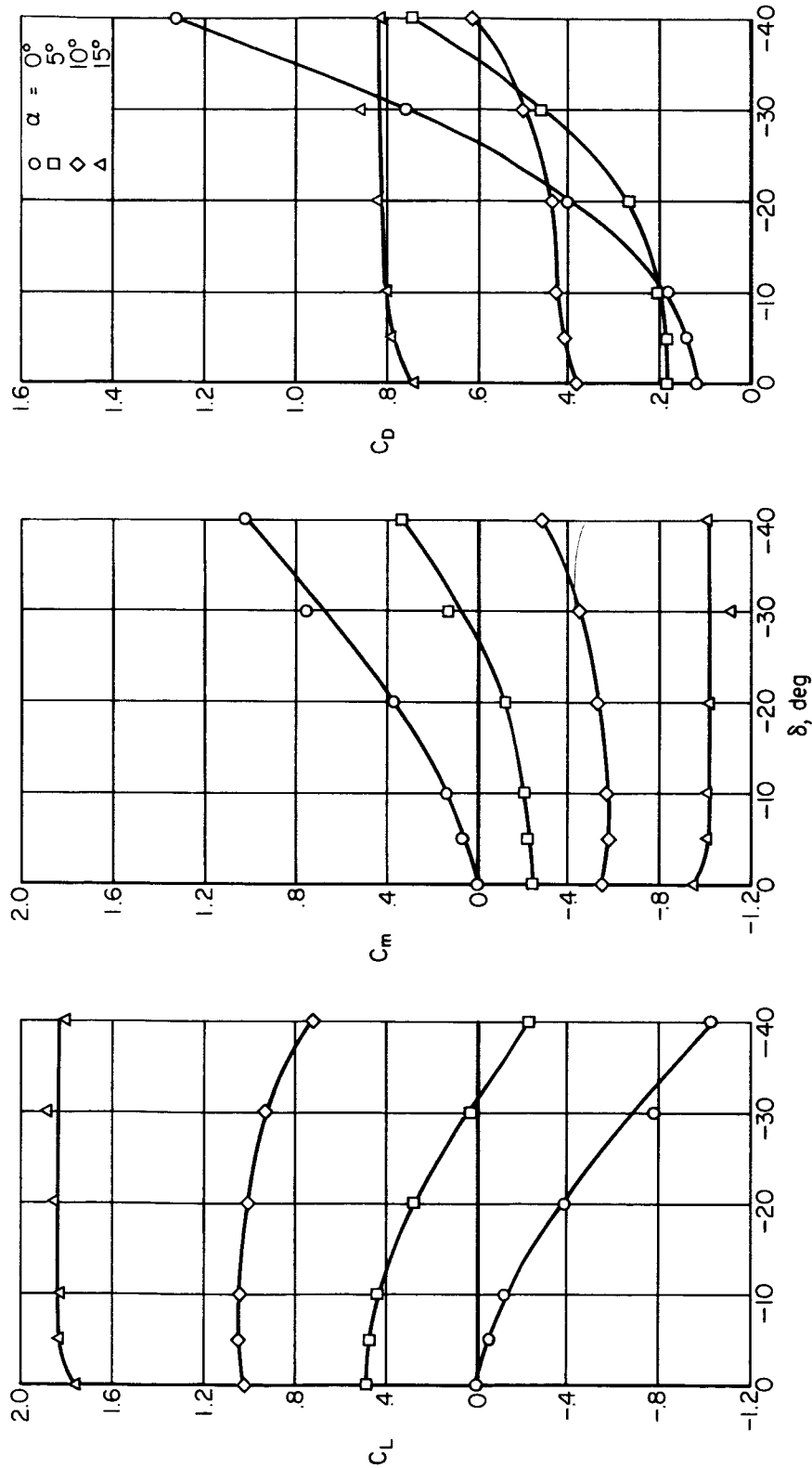
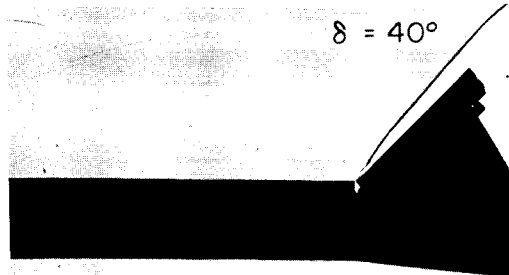
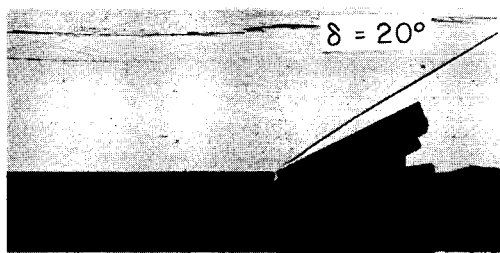
(c)  $M = 5.05$ 

Figure 3.- Continued.

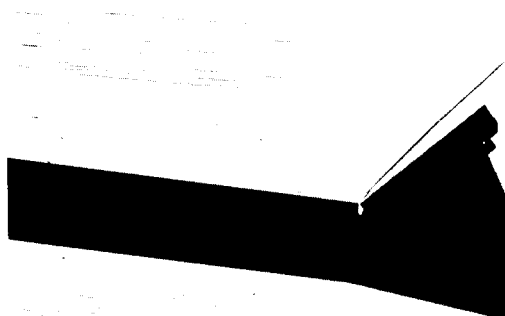
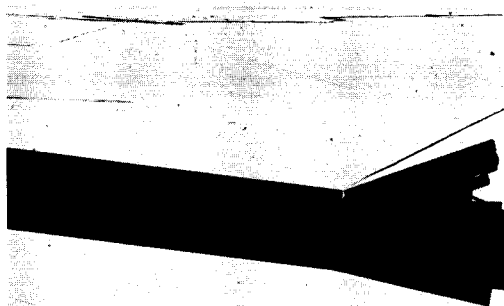


(d)  $M = 6.28$

Figure 3.- Concluded.

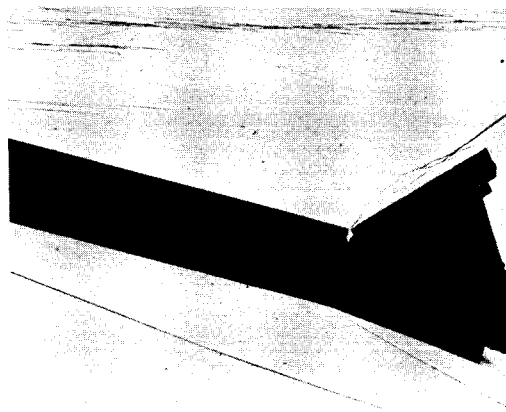
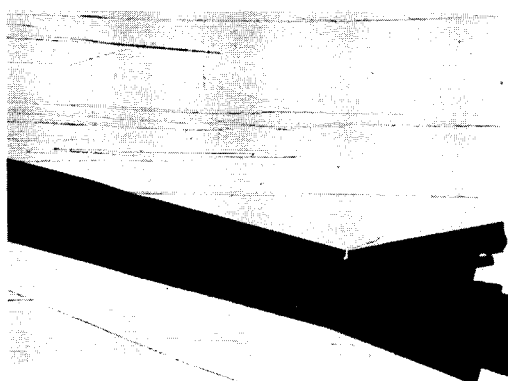


(a)  $\alpha = 0^\circ$ ,  $M = 4.2$



405

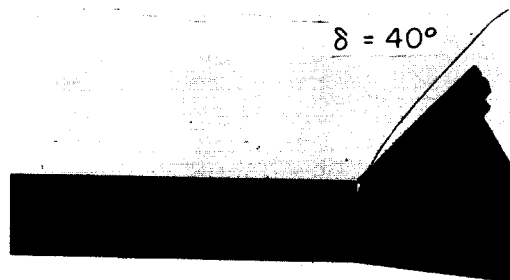
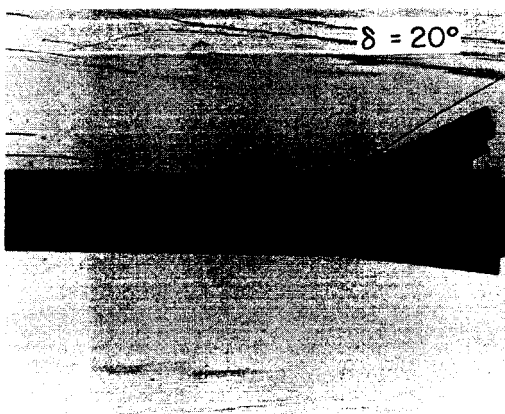
(b)  $\alpha = 7^\circ$ ,  $M = 4.2$



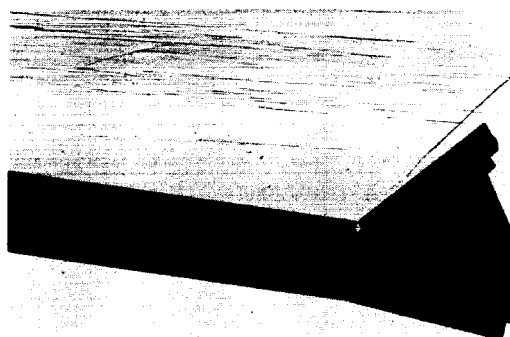
(c)  $\alpha = 14^\circ$ ,  $M = 4.2$

Figure 4.- Spark photographs of the flow in the region of the control.

[REDACTED]

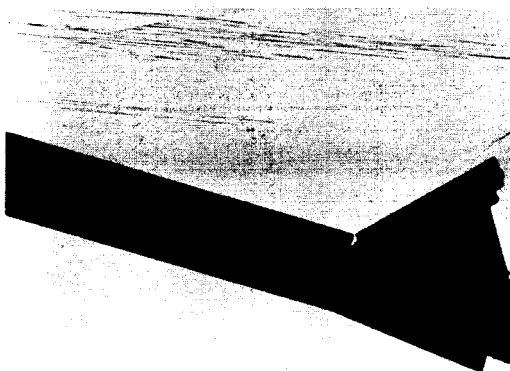
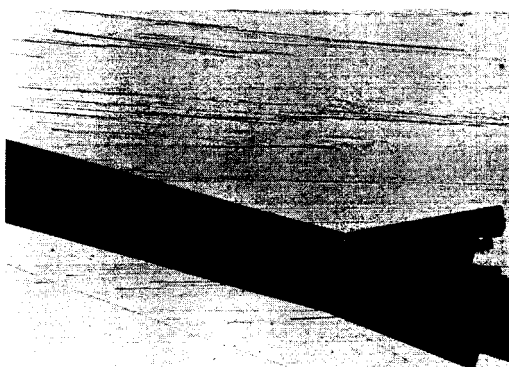


(d)  $\alpha = 0^\circ$ ,  $M = 5.0$



202

(e)  $\alpha = 7^\circ$ ,  $M = 5.0$

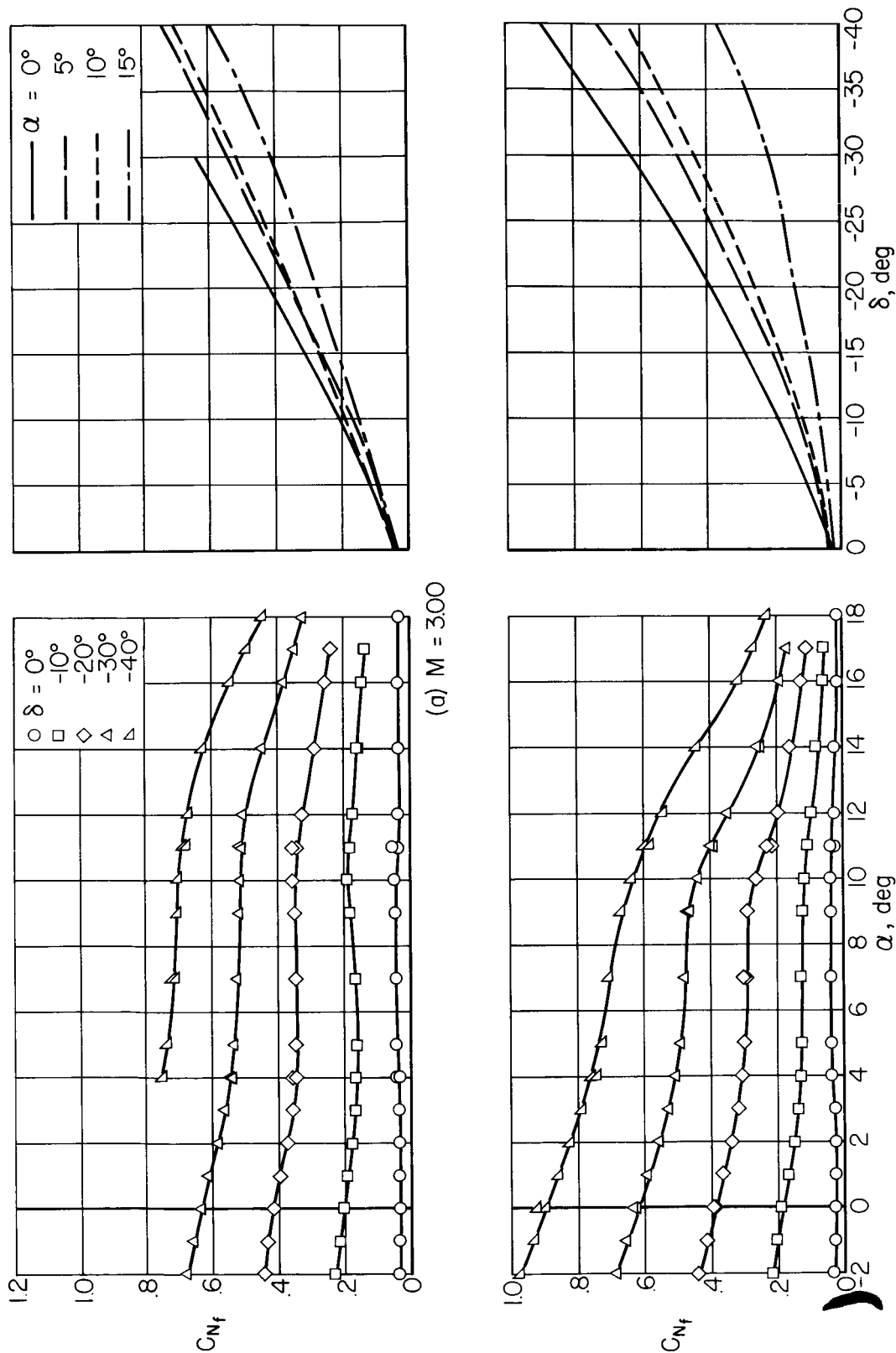


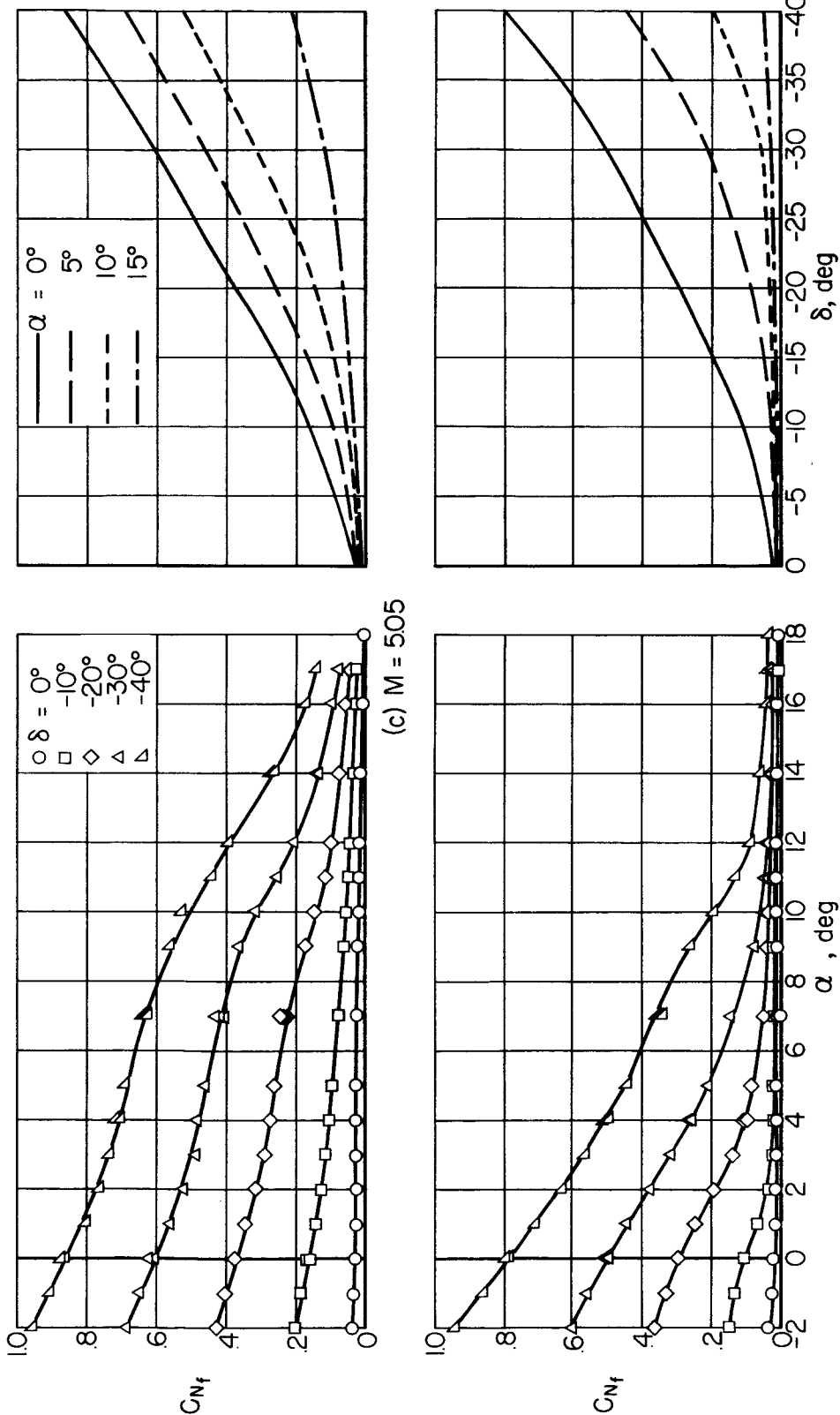
202

(f)  $\alpha = 14^\circ$ ,  $M = 5.0$

Figure 4.- Concluded.



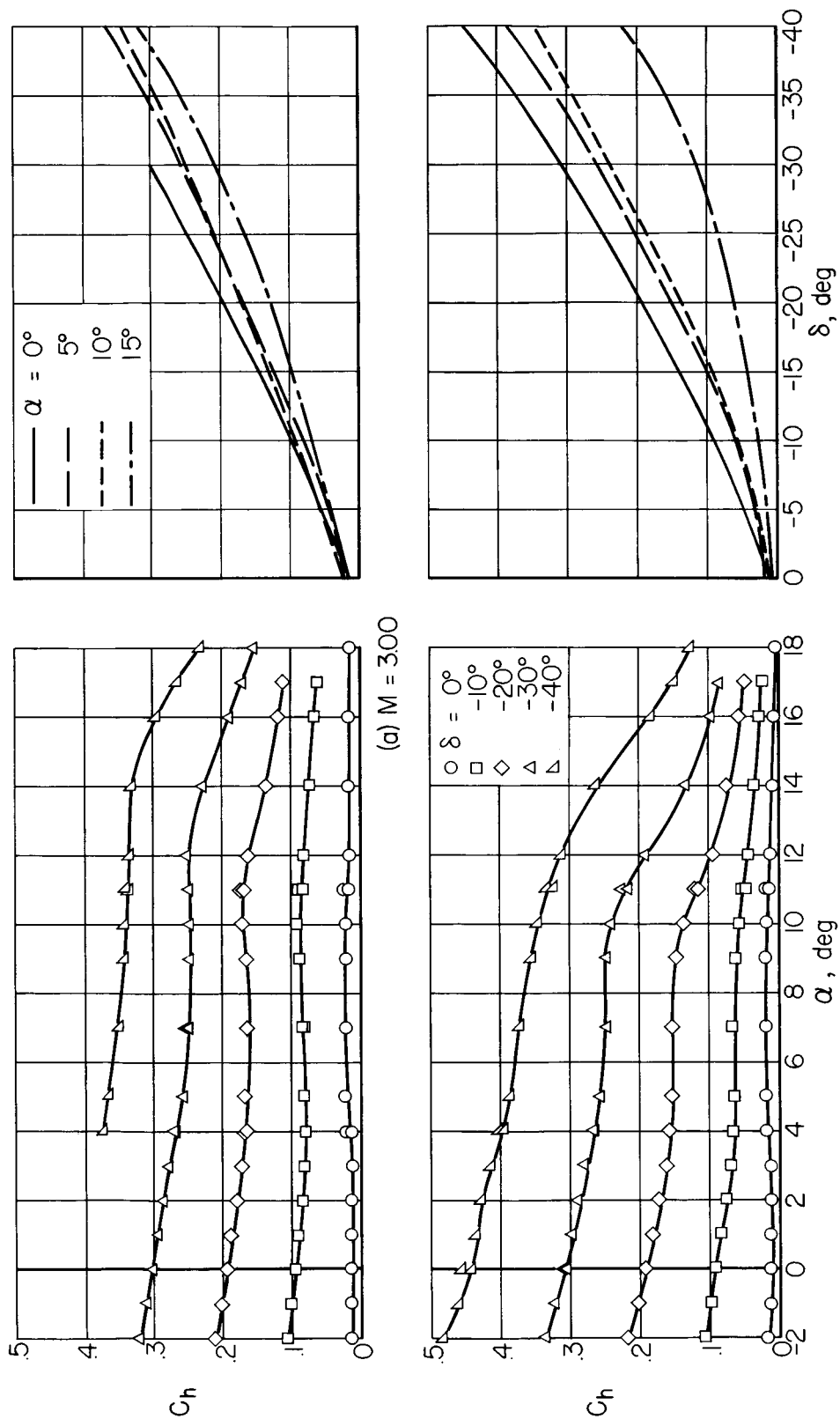
(b)  $M = 4.24$ Figure 5.- Variation of control normal force with  $\alpha$  and  $\delta$ .



(d)  $M = 6.28$

Figure 5.- Concluded.



Figure 6.- Variation of control hinge moments with  $\alpha$  and  $\delta$ .

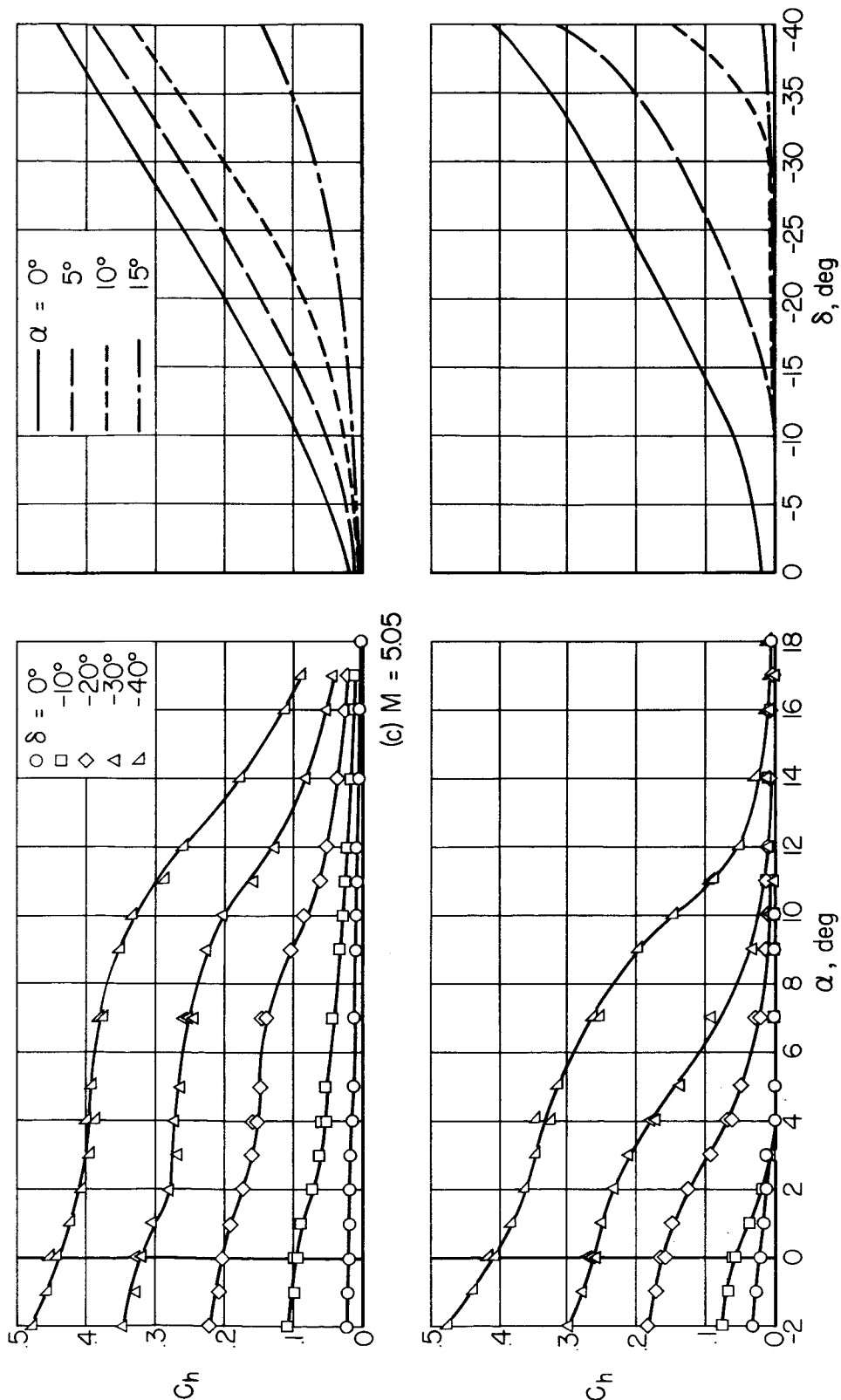


Figure 6.- Concluded.

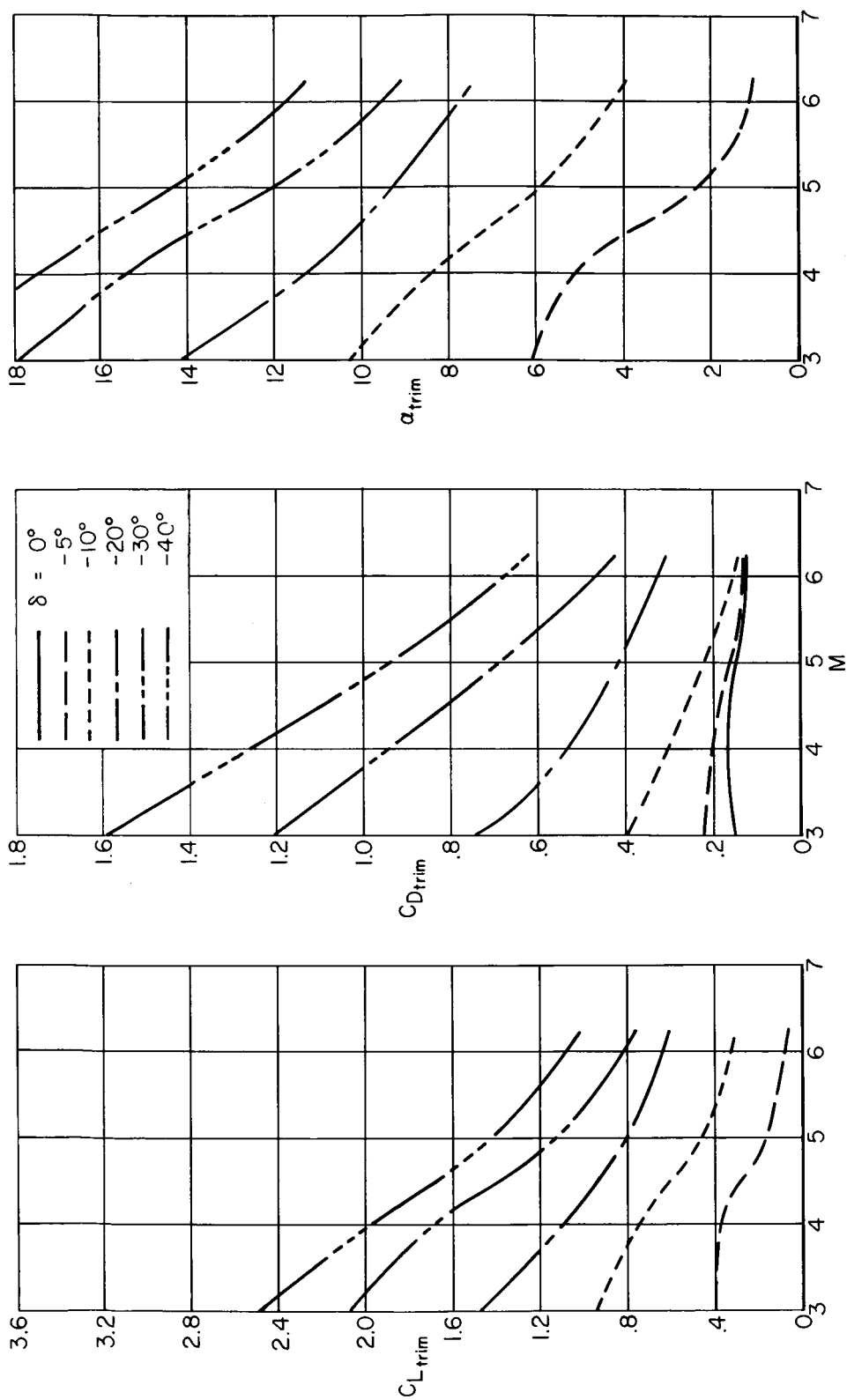


Figure 7.- Variation of trim characteristics with Mach number.

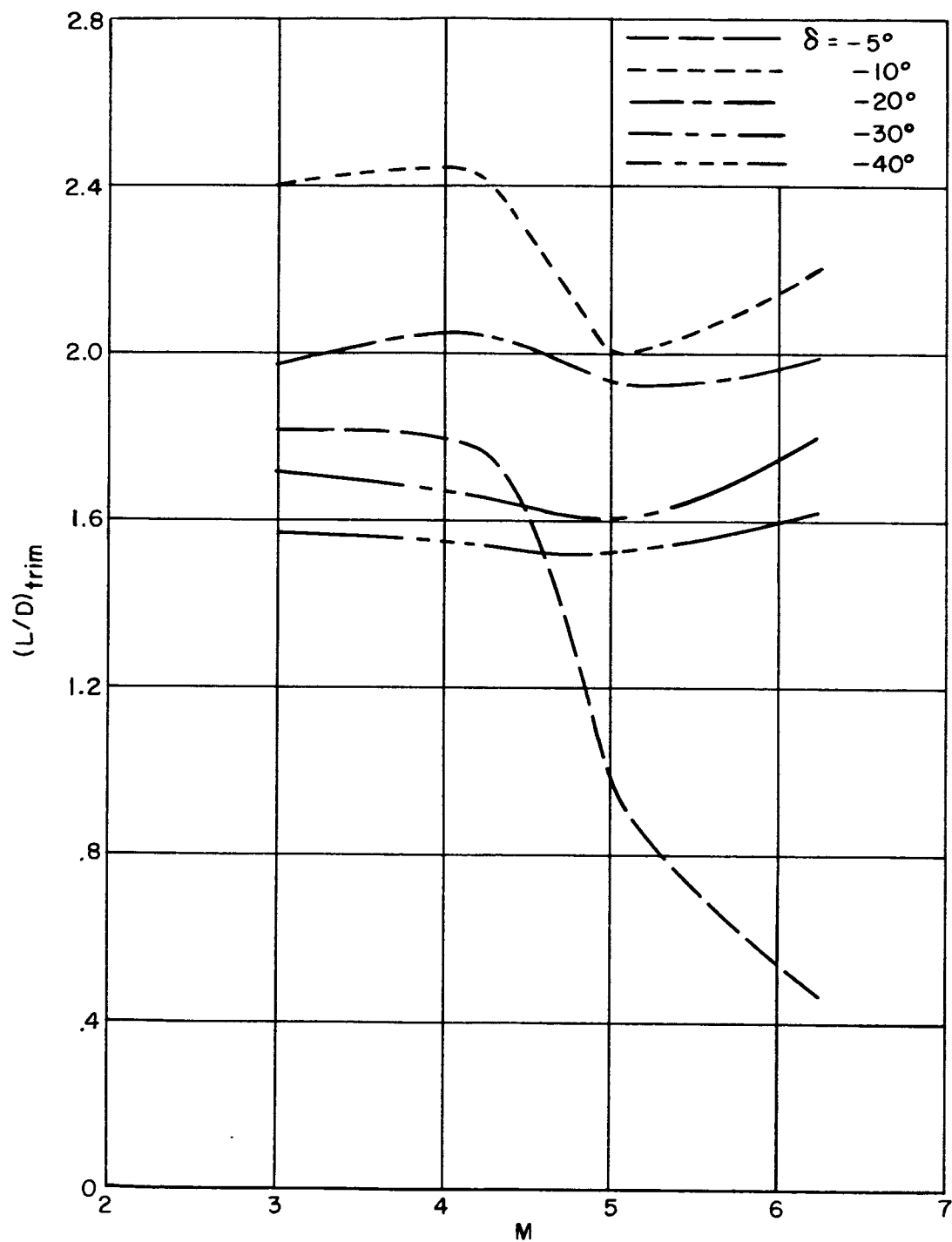


Figure 8.- Variation of trim lift-drag ratios with Mach number.

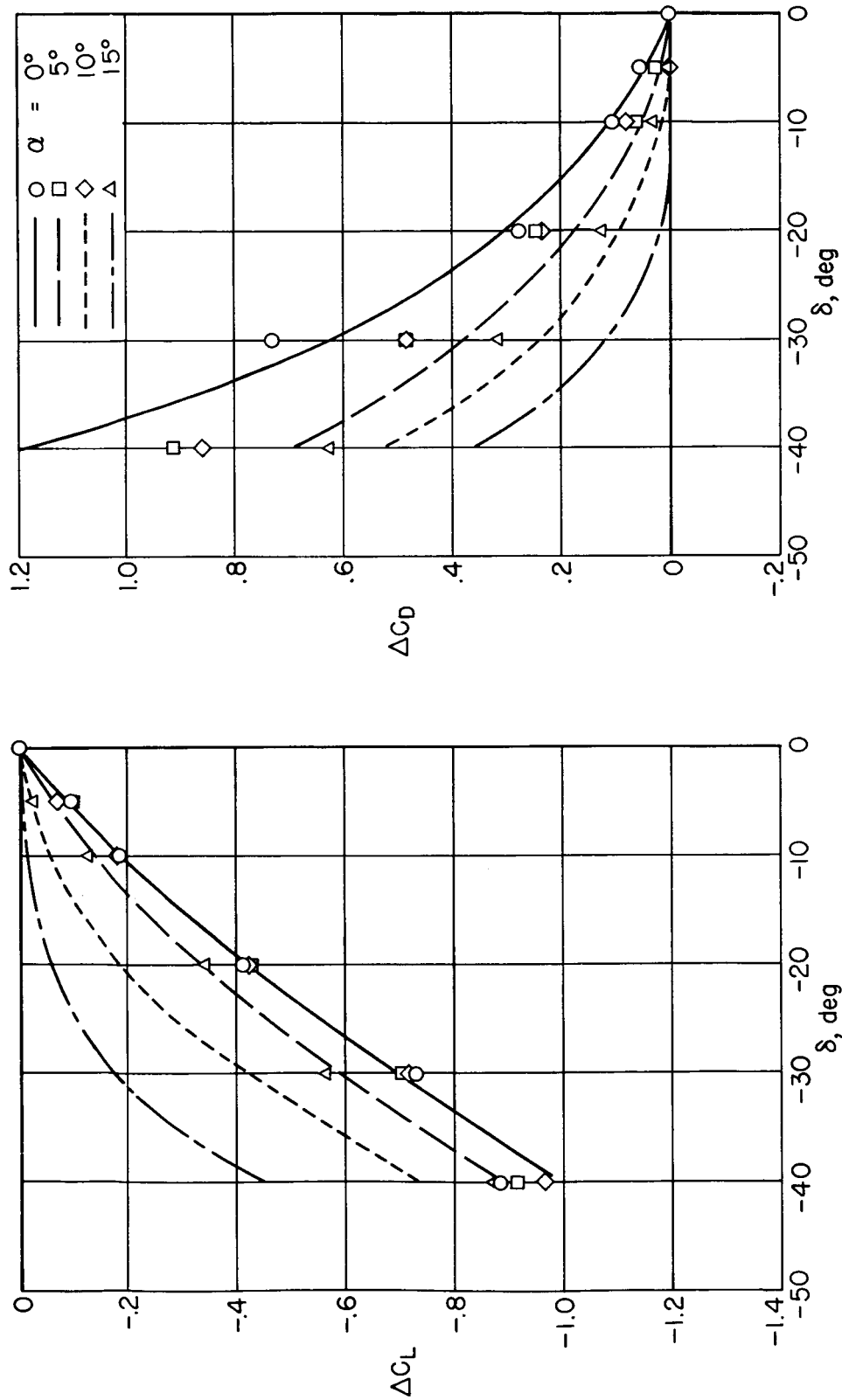
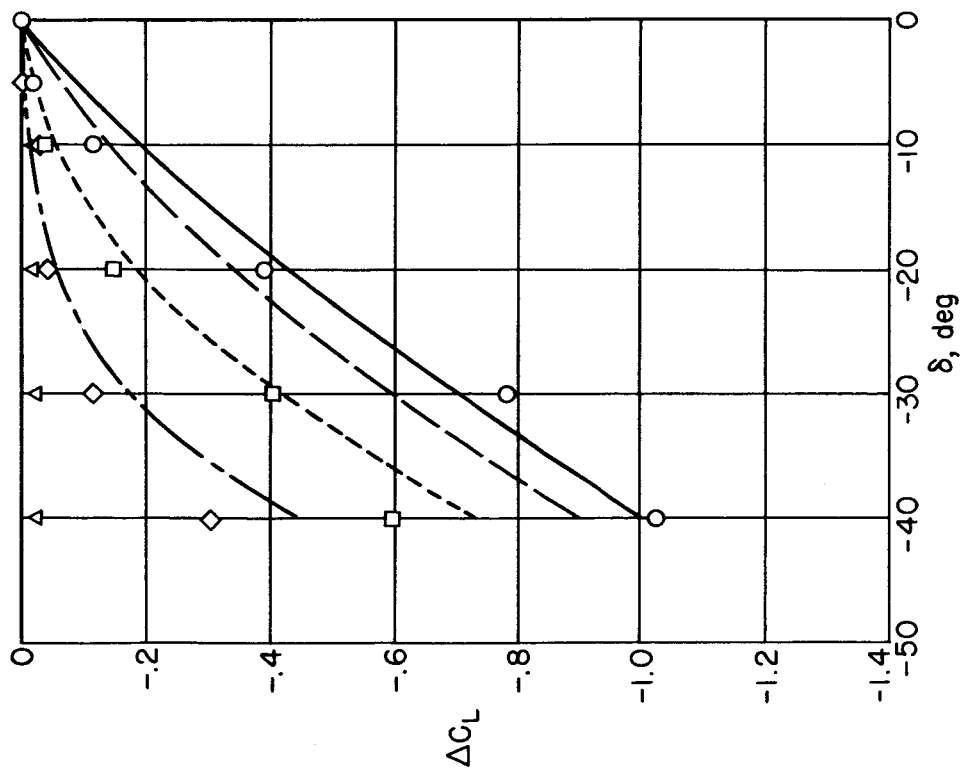
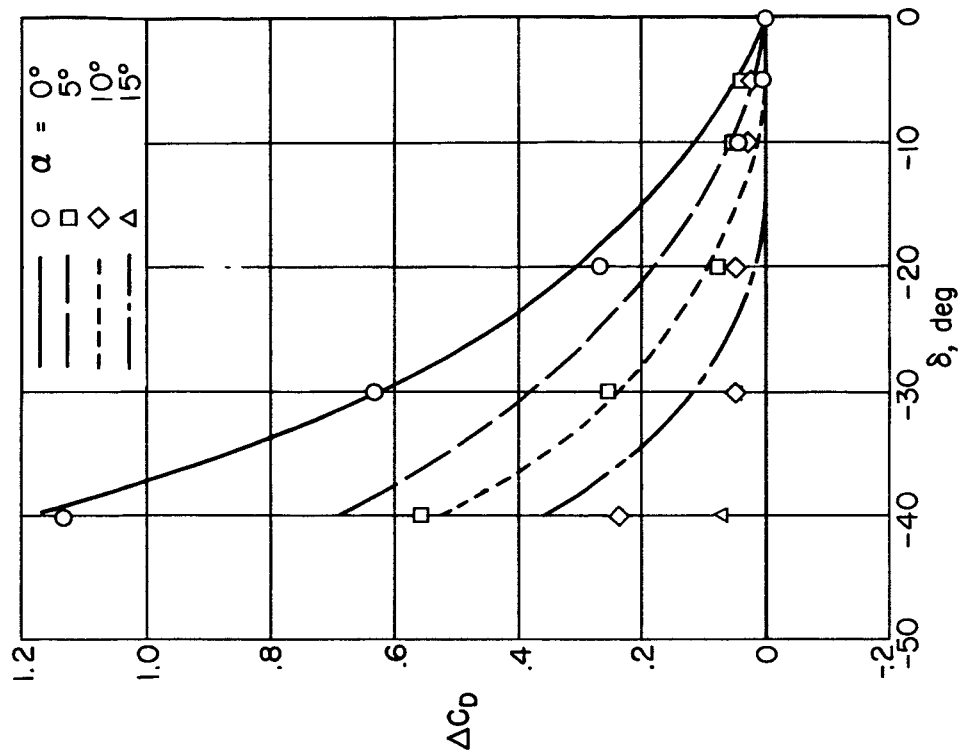
(a)  $M = 3.00$ 

Figure 9.- Theoretical and experimental values of incremental forces due to control deflection.



(b)  $M = 6.28$

Figure 9.- Concluded.